NASA
Technical Memorandum 107198

Army Research Laboratory
Technical Report ARL–TR–876

Application of a Multi-Block CFD Code to Investigate the Impact of Geometry Modeling on Centrifugal Compressor Flow Field Predictions

Michael D. Hathaway
Vehicle Propulsion Directorate
U.S. Army Research Laboratory
Lewis Research Center
Cleveland, Ohio

and

Jerry R. Wood
Lewis Research Center
Cleveland, Ohio

Prepared for the
41st Gas Turbine and Aeroengine Congress
sponsored by the Intertnational Gas Turbine Institute of the
American Society of Mechanical Engineers
Birmingham, United Kingdom, June 10–13, 1996

National Aeronautics and
Space Administration

Application of a Multi-Block CFD Code to Investigate the Impact of Geometry Modeling on Centrifugal Compressor Flow Field Predictions

Michael D. Hathaway
U. S. Army Vehicle Propulsion Directorate
Cleveland, Ohio

Jerry R. Wood
NASA Lewis Research Center
Cleveland, Ohio

ABSTRACT

CFD codes capable of utilizing multi-block grids provide capability to analyze the complete geometry of centrifugal compressors including, among others, multiple splitter rows, tip clearance, blunt trailing edges, fillets, and slots between moving and stationary surfaces. Attendant with this increased capability is potentially increased grid setup time and more computational overhead - CPU time and memory requirements - with the resultant increase in "wall clock" time to obtain a solution. If the increase in "difficulty" of obtaining a solution significantly improves the solution from that obtained by modeling the features of the tip clearance flow or the typical bluntness of a centrifugal compressor's trailing edge, then the additional burden is worthwhile. However, if the additional information obtained is of marginal use then modeling of certain features of the geometry may provide reasonable solutions for designers to make comparative choices when pursuing a new design. In this spirit a sequence of grids were generated to study the relative importance of modeling versus detailed gridding of the tip gap and blunt trailing edge regions of the NASA large low speed centrifugal compressor for which there is considerable detailed internal laser anemometry data available for comparison.

The results indicate: 1) There is no significant difference in predicted tip clearance mass flow rate whether the tip gap is gridded or modeled. 2) Gridding rather than modeling the trailing edge results in better predictions of some flow details downstream of the impeller, but otherwise appears to offer no great benefits. 3) The pitchwise variation of absolute flow angle decreases rapidly up to 8% impeller radius ratio and much more slowly thereafter. Although some improvements in prediction of flow field details are realized as a result of analyzing the actual geometry there is no clear consensus that any of the grids investigated produced superior results in every case when compared to the measurements. However, if a multi-block code is available it should be used as it has the propensity for enabling better predictions than a single block code which requires modeling of certain geometry features. If a single block code must be used some guidance is offered for modeling those geometry features which can't be directly gridded.

NOMENCLATURE

$\hat{g}_m$	Unit vector in local meridional grid direction
J	Streamwise measurement grid index
ccf	Cumulative mass flow through tip clearance gap, kg/sec
cf	Clearance mass flow per unit meridional chord, kg/sec
mf	Inlet mass flow, kg/sec
m/m_s	Non-dimensional shroud meridional distance
P_t	Total pressure, N/m^2
PS	Pressure surface/side
r/r_t	Radius non-dimensionalized by exit tip radius
SS	Suction surface/side
T_t	Total temperature, K
U_t	Impeller speed at trailing edge, m/sec
V_m	Meridional velocity component = $\sqrt{V_z^2 + V_r^2}$, m/sec
V_r	Radial velocity component, m/sec
V_{tf}	Throughflow velocity component = $\vec{V}_m \cdot \hat{g}_m$, m/sec
V_z	Axial velocity component, m/sec
V_θ	Tangential velocity component, m/sec
y^+	Non-dimensional distance from wall
β	Absolute flow angle, deg., $\beta = tan^{-1}[V_\theta/V_m]$
ω	Rotational speed, radians/sec

Subscripts

1	Impeller inlet station
2	Impeller exit station, r/r_t= 1.065
cfd	ADPAC prediction
exp	Measurements

Superscipts

—	Mass averaged

INTRODUCTION

The complexity of realistic turbomachinery fluid dynamic problems routinely challenge the ability of computational fluid dynamic analysis codes to obtain reasonable flow field predictions. As such, good engineering approximations are often required to model those aspects of the problem which either defy direct analysis, unnecessarily complicate the problem, or adversely affect convergence. Often, modeling is required to simplify analyses sufficiently such that CFD predictions can be obtained in reasonable time frames so as to be useful as a design tool. One relatively simple means of decreasing analysis time is to reduce the total number of grid points used to discretize the flow field. Thus, in areas of the flow field where the details of the flow may not be required, such as within the clearance gap of turbomachinery blades, modeling may be used to reduce the total number of grid points. Although this type of modeling is often routine practice, to our knowledge no investigations of the impact of such modeling on the flow field predictions has been reported in the literature.

CFD codes capable of utilizing multi-block grids provide capability to accurately define the complete geometry of centrifugal compressors including, among others, multiple splitter rows, tip clearance gaps, blunt trailing edges, fillets, and slots between moving and stationary surfaces. Attendant with this increased capability is potentially increased grid setup time and more computational overhead - CPU time and memory requirements - with the resultant increase in "wall clock" time to obtain a solution. If the increase in "difficulty" of obtaining a solution significantly improves the solution from that obtained by modeling the features of the tip clearance flow or the typical bluntness of a centrifugal compressor's trailing edge, then the additional burden is worthwhile. However, if the additional information obtained is of marginal use then modeling of certain features of the geometry may provide reasonable solutions for designers to make comparative choices when pursuing a new design. In this spirit a sequence of grids were generated for the NASA Low Speed Centrifugal Compressor (LSCC) for which there is considerable detailed internal laser anemometry data available for comparison.

The CFD code, ADPAC, was chosen for this study. ADPAC is a general purpose time marching three-dimensional Euler/Navier-Stokes aerodynamic analysis code capable of predicting steady and unsteady compressible transonic flows about ducted and unducted propulsion systems employing multiple blade rows.

For this investigation, several grids were generated to determine the relative importance of grid topology on the final solution. Four analyses were obtained: two solutions for conventional single block grids with the tip modelled and two different trailing edge models, a multiple-block solution wherein the blade tip is modelled and a rather coarse trailing edge block is used, and a multiple-block solution wherein detailed grids for the main channel, tip, and trailing edge blocks were used. The resulting solutions were then compared to assess the relative importance of the various modeling schemes on the final solution obtained, as well as the benefits and costs relative to CPU time and memory requirements of single versus multi-block analyses. The laser anemometer results are included for comparison to provide a degree of reality for assessing the absolute measure of a solution's worth.

TEST COMPRESSOR AND MEASUREMENT TECHNIQUE

The test compressor is a backswept impeller which has 20 full blades with a backsweep of 55° from radial. The compressor was tested at a mass flow rate of 30 kg/sec (66 lbm/sec) at a corrected shaft speed of 1862 RPM. The inlet diameter is 870 mm and the inlet blade height is 218 mm. The exit diameter is 1524 mm and the exit blade height is 141 mm. The tip clearance between the impeller blade and the shroud is 2.54 mm and is constant from inlet to exit. This tip clearance is 1.8% of blade height at the impeller exit and 1.2% at the inlet. The blade surfaces are composed of straight-line elements from hub to tip. A vaneless diffuser was used for the laser anemometer investigation. This allows an axisymmetric boundary condition to be used in the numerical simulations. A complete description of the facility can be found in Wood et al. (1983) and Hathaway et al. (1992). Hathaway et al. (1993) and Chriss et al. (1994) give a detailed presentation of the laser data which is summarized below.

The measurement results consist of standard 5–hole pneumatic probe surveys and torque measurements for performance characteristics, and detailed laser anemometer surveys of the impeller flow field. A two-component laser fringe anemometer operating in on-axis backscatter mode was used in the experiment. In order to obtain all three velocity components, two sets of measurements were obtained, each at a different orientation to the flow. The resulting four measured velocity components were then combined with a least squares fit in order to obtain the three components of velocity.

The laser anemometer surveys are shown in Fig. 1, and the streamwise indices of the body-fitted grid at which the laser surveys were acquired are noted together with the percent meridional shroud distance of survey planes within the impeller and radius ratio of survey planes within the vaneless diffuser. The streamwise indices corresponding to the leading and trailing edges are 51 and 171, respectively.

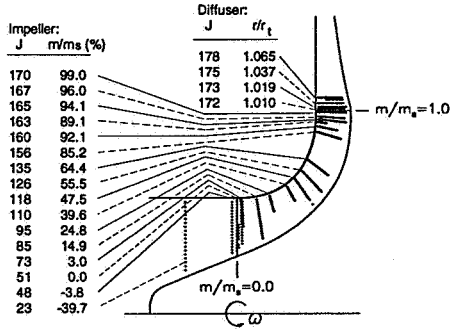

Figure 1 Laser anemometer survey station locations.

All the data are ensemble-averaged across the 20 blade channels to yield a single "representative" blade passage. This passage is divided into 1000 equal arc lengths or window "bins." For presentation purposes these bins are usually averaged down to 200 measurement locations across the blade passage.

An estimate of the uncertainty in the calculated results was made from the least squares fit calculations. Throughout most of the impeller passage the uncertainty is estimated to be ±1.5 m/s, which is about 2% of the through-flow velocity, although the uncertainties can approach 15% in the through-flow wake near the impeller exit.

Further details of the philosophy and the method used to obtain and average the data can be found in Strazisar et al. (1989). Complete documentation of the aero and laser data acquisition and reduction

procedures, including documentation of all data acquired during the low speed centrifugal compressor program, can be found in Hathaway, et al (1995).

CFD ANALYSIS APPROACH

The computational results for the LSCC flow field were obtained using the Advanced Ducted Propfan Analysis Code (ADPAC) developed by Allison Engine Company under NASA contract (Hall and Delaney 1992, Hall et al. 1994). ADPAC is a general purpose time-marching three-dimensional Euler/Navier-Stokes aerodynamic/heat transfer analysis tool for predicting steady and unsteady compressible transonic flows within modern turbomachinery propulsion systems employing multiple blade rows. ADPAC is based on a flexible multiple-block grid discretization scheme permitting coupled 2–D/3–D mesh block solutions with application to a wide variety of geometries. Aerodynamic calculations are based on a four-stage Runge-Kutta time-marching finite-volume cell-centered technique with added numerical dissipation. Steady flow predictions are accelerated by a multigrid procedure. ADPAC is capable of either serial execution or parallel execution on multiple workstations or other CPU's.

Numerical Technique

The numerical solution procedure is based on an integral representation of the strong conservation law form of the Navier-Stokes equations expressed in a cylindrical coordinate system. The discrete numerical solution is developed from the integral governing equations by employing a finite-volume cell-centered solution procedure. This procedure closely follows the basic scheme described by Jameson et al. (1981). The numerical technique is second order accurate in space using central differences for flux evaluations. The discretized system of equations has unstable properties and can exhibit odd-even decoupling. To suppress these instabilities, artificial dissipation terms made up of second and fourth order difference operators are added to the equations. The time stepping scheme used to fully discretize the system of equations is a four-stage Runge-Kutta integration. Local time stepping for each cell and residual averaging is used to accelerate the convergence of steady flow analyses. Turbulent stresses are simulated using the model of Baldwin and Lomax (1978). For all calculations presented herein, wall functions were used whenever ADPAC determined the near wall mesh spacing was greater than a y^+ of 10.0.

In multi-block grid systems such as is employed by ADPAC the domain of interest is subdivided into one or more structured arrays of hexahedral cells. Each array of cells is referred to as a "block", and the overall scheme is referred to as a multiple blocked mesh solver as a result of the ability to manage more than one block. A multiple blocked grid system has advantages over a single block grid as it is not often possible to generate a single structured grid to encompass the domain of interest without sacrificing grid quality. Unstructured grid codes, of course, provide another alternative. Multiple block grid systems differ from single block grid systems only in that the numerical solution is generated from multiple computational domains (blocks). ADPAC utilizes the multiple blocked grid concept to full extent by permitting an arbitrary number of structured grid blocks with user specifiable communication paths between blocks. The inter-block communication paths are implemented as a series of boundary conditions on each block which, in some cases, communicate flow information from one block to another.

All solid surfaces must satisfy flow tangency for inviscid flow and, in addition, no slip for viscous flows. In both cases, no convective flux through the boundary (an impermeable surface) is permitted. These conditions are satisfied by using a phantom cell located outside of the computational domain for each cell which touches a solid boundary. The phantom cell velocity components are thus constructed to ensure that the cell face average values used in the convective flux calculation are identically zero. The phantom cell pressure is simply extrapolated based on the boundary layer flow concept that the normal pressure gradient is zero at the wall.

Inflow and exit boundary conditions are applied numerically using characteristic theory. For subsonic normal inflow, the upstream running Reimann invariant is extrapolated to the inlet and the flow variables at the boundary are determined using the equation of state along with the specified total pressure, total temperature, and radial and circumferential flow angles. Outflow boundaries require a specification of the exit static pressure at either the top or bottom of the exit plane. The remaining pressures along the outflow boundary are calculated using simple radial equilibrium, which for the LSCC, results in a constant static pressure since the exit boundary is at a constant radius. In this case the downstream running invariant is used to update the phantom cells at the exit boundary.

Artificial damping is applied at the block boundaries by prescribing zero dissipation flux along block boundaries to maintain the global conservative nature of the solution for each mesh block. Fourth order dissipation fluxes at near-boundary cells are computed using a modified one-sided difference scheme. Implicit residual smoothing is applied at the block boundary by imposing a zero residual gradient condition at the boundary. For the multiple-block scheme, the solution is performed on a single block at a time. Therefore, special boundary conditions are required along block boundaries to provide for transport of information between blocks. For all meshes presented herein the neighboring mesh blocks have coincident mesh points along the interface separating the blocks. Therefore, a simple direct specification of the phantom cell based on the near-boundary cell data from the neighboring block is employed. In other words, each phantom cell in the block of interest has a direct correspondence with a near-boundary cell in the neighboring mesh block, and the block coupling is achieved numerically by simply assigning the value of the corresponding cell in the neighboring block to the phantom cell in the block of interest. This procedure essentially duplicates the interior point solution scheme for the near-boundary cells, and uniformly enforces the conservation principles implied by the governing equations.

Computational Grids

As previously mentioned, the purpose of this investigation was to assess the impact of detailed gridding versus modeling of the tip gap and trailing edge on the computational predictions, as well as the benefits and costs in terms of CPU time and memory requirements. As such, several grids were generated using computer codes developed by Wood (1994) to determine the relative importance of grid topology on the final solution. Four analyses were obtained: two solutions for conventional single block grids with the tip modelled and two different trailing edge models, a multiple-block solution wherein the blade tip is modelled and a rather coarse trailing edge block is used, and a finer mesh multiple-block solution wherein detailed grids for the main

channel, tip, and trailing edge blocks were used. Table 1 provides a comparison of the various grids analyzed and Fig's. 2 and 3 illustrate the differences in the gridding for modeling versus blocking the tip gap and trailing edge of the LSCC. The mesh sizes quoted in table 1 are the number of streamwise, spanwise, and pitchwise nodes, respectively. Sheared H-grids were used for all cases presented herein with the exception of the leading edge tip gap region which used a modified C-grid. Inspection of the LSCC blade tips indicated that the tips are slightly rounded at each corner. We therefore assumed that there would be no vena-contracta in the tip gap flow as would exist for sharp-edged tips, and that a discharge coefficient of 1.0 is appropriate for the tip gap flow (Chriss, et al, 1994). Therefore, the full physical gap height was used for all computations. However, each model incorporates a square edge tip rather than the "true" rounded tip corners.

Table 1 Comparison of modeling differences and mesh sizes of various mesh configurations analyzed.

		MESH CONFIGURATIONS STUDIED			
	Block Structure	Single Block		Multiple Block	
	Case	S	M	C	F
	Tip Model	Yes	Yes	Simulated	Mesh Block
	T.E. Model	Tapered to mean camber line	Suction side tapered to pressure surface	Mesh Block	Mesh Block
Mesh Size	Main Block	129×61×41	129×61×41	129×61×41	155×71×51
	Tip Block	N/A	N/A	75×5×9	101×11×21
	T.E. Block	N/A	N/A	29×61×13	29×71×21
	Total Nodes	322,629	322,629	349,001	628,936
	Ratio	1.000	1.000	1.082	1.949

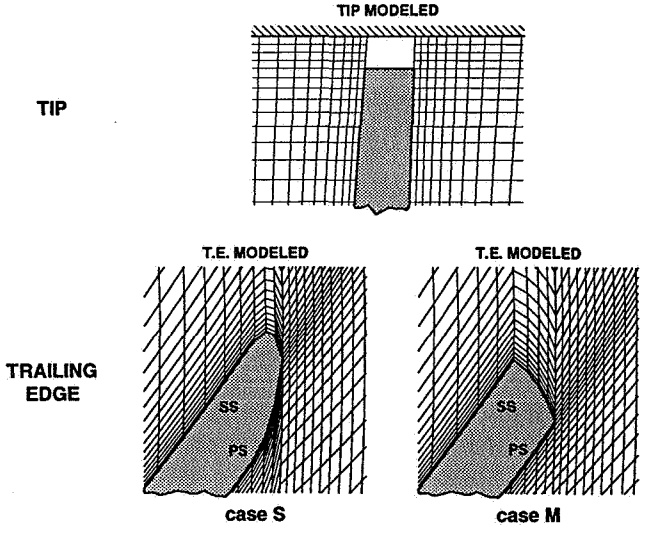

Figure 2 Single block meshes.

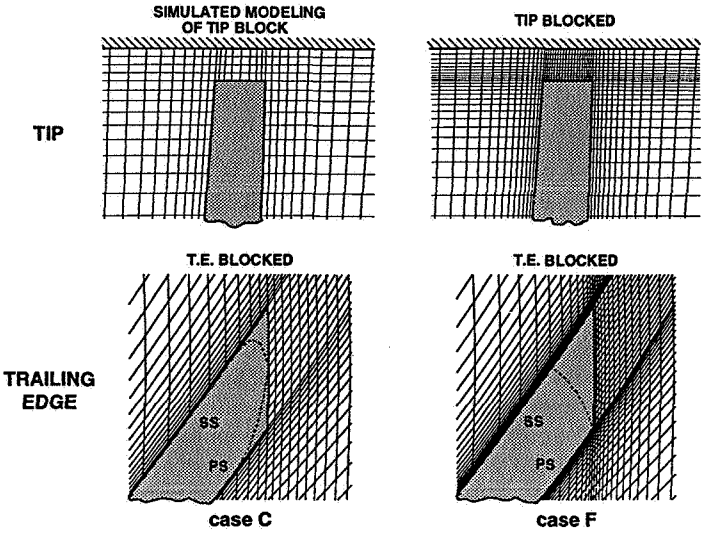

Figure 3 Multi-block meshes.

The single block case S models the trailing edge by quadratic curves blending the suction and pressure surfaces to the trailing edge at the mean camber line point. The single block case M uses a quadratic curve to blend the suction surface to the trailing edge with no modification of the pressure surface. For both cases S and M the trailing edge modifications occur over the last 1.5% of meridional chord from the trailing edge (78% of the mid-span trailing edge thickness).

The trailing edge model of case M was guided by the observed differences in flow turning near the trailing edge as shown in Fig. 4. Figure 4 shows that the flow near the trailing edge of the single block case S is under-turned relative to the multi-block cases C and F. This under turning is being driven by the pressure surface curvature which results in the pressure surface flow driving the flow towards the suction side and thus under turning the flow relative to that predicted by the multi-block cases which accurately model the trailing edge geometry. As a result, the trailing edge modeling of case M was accomplished by following the suggestion of Adamczyk (1995) which he has employed in the past in order to alleviate the tendency of compressor trailing edges to under turn as a result of inadequate modeling of the trailing edge details. By cutting back the suction surface the tendency of the suction surface flow to be "pushed back" by the pressure surface flow is reduced.

Both case S and M model the blade clearance gap by a squared off tip at the physical blade tip wherein the pressure and suction surface grids are separated by the physical blade thickness and their respective boundary conditions across the clearance gap are forced to be reflective (i.e., the phantom cells along the suction surface boundary are substituted with the flow variables from the adjacent pressure surface boundary and vice versa). The supposition behind this approach is that the details of the flow through the clearance gap are not necessary so long as the correct amount of flow is allowed to pass through the clearance gap. Previous analysis of the LSCC impeller reported in the literature tend to support this supposition (Chriss, et al. 1994).

Cases C and F feature a trailing edge block that grids the true blade trailing edge geometry, which is truncated at the impeller exit radius. Grid block matching requirements in the clearance gap at the trailing

edge dictated that we add a grid block over the blade tip when the trailing edge block was added. In an attempt to separate the differences in the predictions resulting from the tip and trailing edge blocks, the blade tip and casing surface boundaries of the tip block are treated as inviscid boundaries for the coarse multiple block case C. The clearance flow treatment for case C is therefore quite similar to that for cases S and M and differences between these three cases should be due mainly to trailing edge treatment variations. The finer mesh multi-block case F allows the blade tip and casing boundaries of the clearance gap mesh block to be viscous so as to allow the CFD code to predict "blockage" through the clearance gap. Case F also features a sizable increase in grid density in the tip mesh block and moderate increases in grid density in the main and trailing edge blocks.

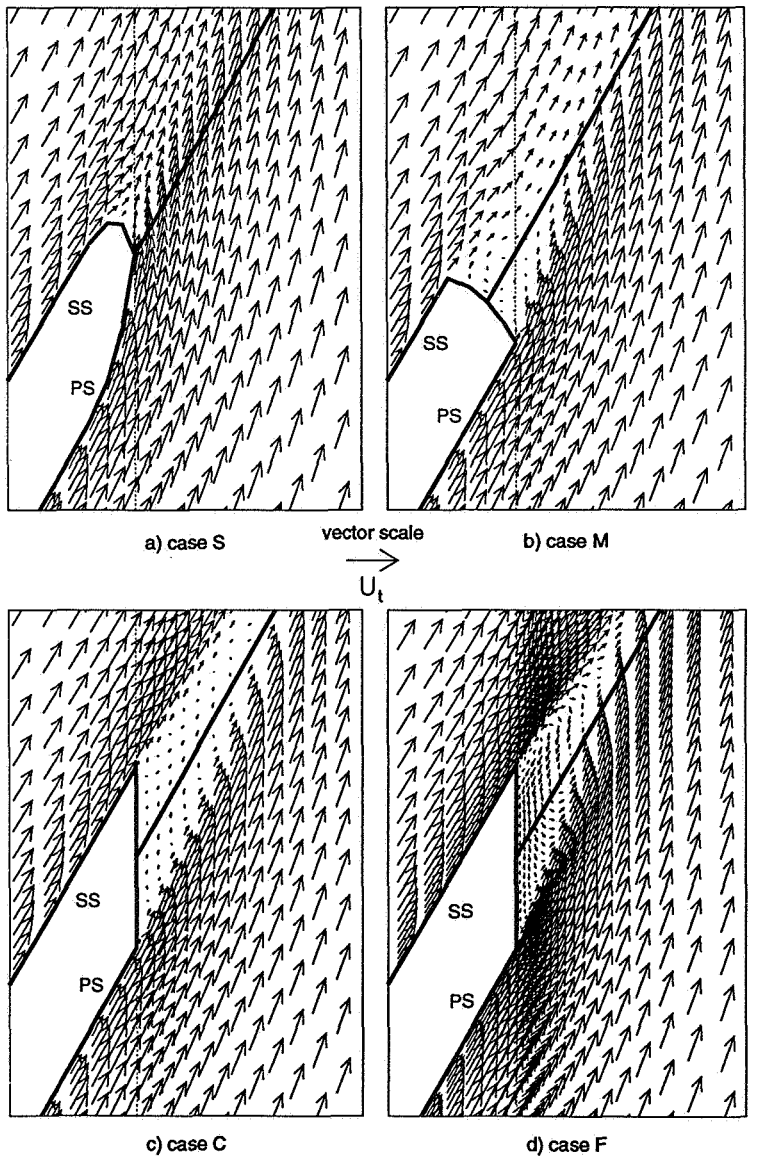

Figure 4 Comparison of predicted relative velocity vectors showing effect of trailing edge modeling on flow turning at mid span.

The mesh for both single block cases and the coarse multiple block case are identical with the following exceptions: The suction side tapering for case M results in slight local changes in the mesh relative to the case S mesh which are commensurate with the different trailing edge modeling. The coarse block case C includes a tip block which fits within the modelled tip gap of case S and a trailing edge block which results in pitchwise redistribution of the main block mesh downstream of the trailing edge relative to case S. To insure good definition of the blade leading edge a C grid was used for the tip block which has coincident sides at the blade mean camber line. The fine block mesh, case F, in addition to providing increased meshing, redistributes the spanwise mesh to insure that the main block mesh smoothly transitions to the spanwise spacing of the tip block mesh near the blade tip. As a result, the fine mesh case is actually slightly coarser away from the hub and casing (roughly from 10 to 85% span) than in the coarse mesh case. This decreased spanwise grid density away from the blade end walls is partly responsible for some of the observed differences between fine and coarse mesh predictions, as will be discussed later. The maximum spanwise mesh spacing for case F is 9% of span at 65% span relative to 5.5% of span at 55% span for all other cases. It would be desirable to achieve the same spanwise spacing, but satisfying that condition as well as the others imposed would have increased the grid size by 25% to 788,000 points.

Boundary Conditions and Convergence

For all cases studied the same inlet boundary conditions were imposed based on 5-hole probe survey data, and the exit back pressure was adjusted to achieve the desired mass flow rate. For the comparisons to detailed flow field measurements presented herein, all predictions were converged to the tested mass flow rate, 30 kg/sec. Convergence was determined when the maximum residuals were reduced by at least 3 orders of magnitude and the inlet and exit mass flow, pressure ratio, efficiency, and number of separated points were all converged and stable for at least twice the number of iterations required for these parameters to stabilize after a given perturbation in back pressure.

RESULTS AND DISCUSSION

Since our focus is to illuminate differences in the CFD solutions obtained by modeling certain geometrical features (rather than constructing a computational grid that faithfully reproduces those features) we have assumed the baseline for our comparisons to be the solutions from grid case C. Since the measured laser data provides a degree of reality for assessing the absolute measure of a solution's worth, we have also included it for comparison. As will be seen in the following discussion, in comparisons of the solutions to the measured data there is no clear consensus that any of the grid cases studied provides predictions that are clearly superior to those of the other grid cases. Although one metric may indicate better agreement with the data for one grid case, another metric may indicate better agreement with a different grid case. In our opinion, the relative differences between the various cases studied herein would translate to the same relative degree of differences if we had used a different turbulence model, grid topology, increased grid density, etc.

In comparing the results of the various analyses their ability to predict the compressor overall performance is considered first. Secondly, the axisymmetric averaged exit profiles are compared to determine differences resulting from the detailed gridding versus modeling which

might impact the design of the impeller or downstream diffuser. Next, a comparison of blade-to-blade flow field features such as the blade wake, characteristic through-flow wake (formed by the accumulation of low momentum fluid which migrates to the blade tip and is entrained in the tip clearance vortex), and other secondary flow features at the exit of the impeller is provided to indicate potential improvements in impeller designs to minimize loss production. Finally, the relative costs in terms of CPU time and resources required are assessed to determine if the additional costs incurred are worth the benefits gained.

Comparisons between cases S and M, which model the physical geometry, show the impact of modifications to the trailing edge taper (modeling) which are made over the last 1.5% of meridional chord from the trailing edge. Comparisons of case C to cases S and M show the impact of using a multi-block code to correctly define the blunt trailing edge geometry of the LSCC impeller and also grid the tip gap. Case F shows the impact of increased mesh density in some areas (e.g., case F has over six times as many grid nodes as case C in the tip gap region) and a viscous treatment of the flow through the tip clearance gap.

Overall Performance

Figures 5—7 give a good indication of the differences produced by the four grids from a one dimensional perspective. The predicted performance characteristics for the tested operating conditions are compared in Fig. 5 and show considerable variation in efficiency and overall pressure ratio. The two single block solutions, cases S and M, predict pressure ratios that differ by ±0.5% from the multi-block predictions from grid C which agrees quite well with the experimental pressure ratio data. The single block grid M over-predicts pressure ratio by an almost equal amount that S under-predicts. The finer multi-block grid F differs very little from C and agrees no better with the data even though the number of grid points is nearly doubled. For all cases, the slopes of the predicted overall pressure ratio and efficiency characteristics are in good agreement with the measurements. However, the predicted efficiencies are 3-5 points higher than measured. Grids S, C, and F predict, essentially, the same efficiency curve although they produced slightly different overall pressure ratios. (Note: The uncertainties in the measured torque based efficiency, and adiabatic efficiency based on probe surveys, are 0.5 points and 2 points, respectively.)

The observed differences in predicted pressure ratio of the various cases was investigated further by calculating the predicted meridional distribution of energy averaged pressure rise and mass averaged temperature rise (work input) relative to that based on measured values at the impeller exit, as shown in Fig. 6. Up to about 95% meridional chord all cases predict essentially the same pressure rise (within 0.5% up to 70% meridional chord, and within 1.4% up to 95% meridional chord). At about 85–90% meridional chord the four cases begin to diverge. Figure 6b shows that the reduction in overall pressure rise of case S is predominantly due to under prediction of the overall work input. The increased overall pressure rise of case M resulted from additional work input as a direct result of the different trailing edge modeling. The local turning of the flow around the trailing edge is evident in Fig. 4 where the under-turning of grid S and the slight over turning of grid M near the suction surface is consistent with the pressure rise difference. A comparable plot of the efficiency (not shown)

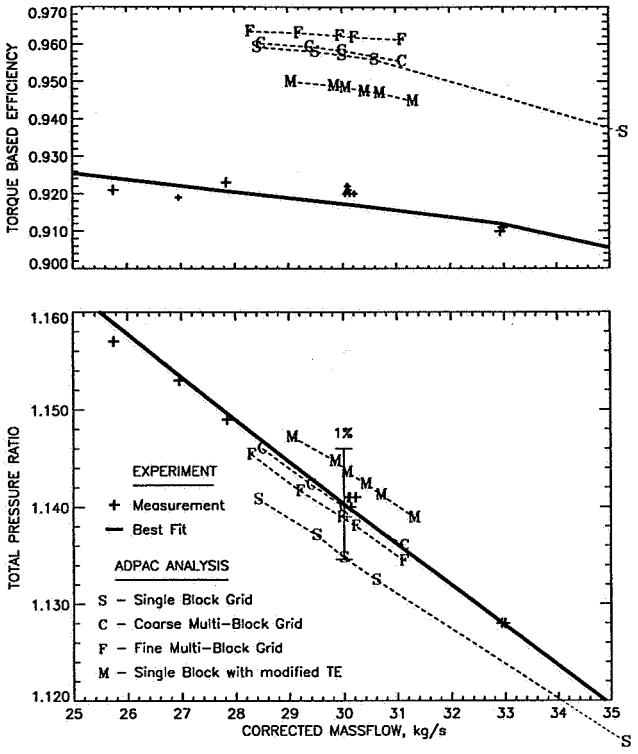

Figure 5 Comparison of predicted and measured performance maps for the large low speed centrifugal impeller.

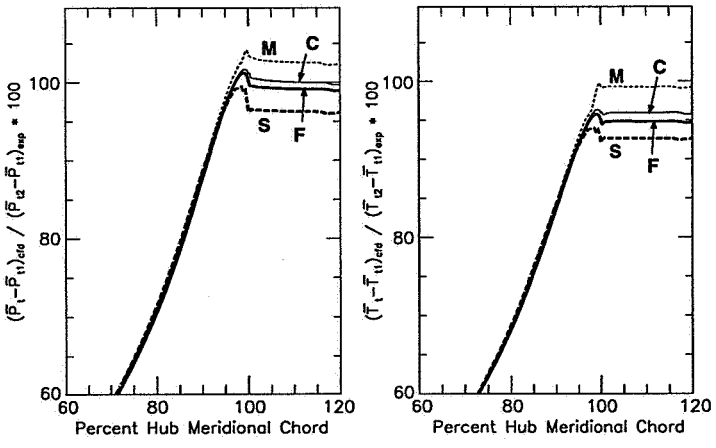

a) Pressure rise **b) Work input**

Figure 6 Comparison of meridional distributions of mass averaged pressure rise and work input through the impeller normalized by their respective measured values.

indicated that the predicted efficiencies using grids S, M, and F are virtually identical at 98% chord whereas grid C is about 0.3 points lower (97.4% to 97.1%). However, from 98% chord to 106% chord, the efficiency for cases S, M, C, and F decrease by 1.5, 2.3, 1.1, and 0.9 points, respectively. The entropy rise up to 96% chord for grids S, M, and F is about 10% lower than for grid C. However, from 96% chord to 102% chord (which includes the taper region of the blade trailing edge

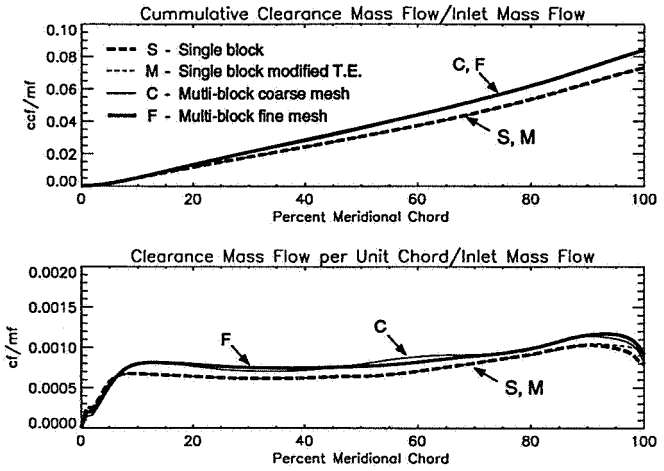

Figure 7 Comparison of predicted meridional distributions of clearance mass flow.

for the single block grids and the dump loss for the blocked grids) the entropy rise for cases S, M, and F are 1.7, 2.8 and 1.0 times as great as for case C. Obviously, the trailing edge treatment has considerable impact upon entropy production as well as work input.

Although the tip clearance gap is handled quite differently for the single block grids and the multi-block grids, the only discernible difference in the solutions for S, M and C at 98% chord is 0.3 points in efficiency for the C grid below the other two. The local and cumulative clearance flows for the four cases are shown in Fig. 7. Grids C and F yield the same overall clearance flow (8.4% of the inlet flow) which is about 1% of inlet flow higher than that obtained with the single block grids which model the tip gap. Grids C and F also give virtually identical distributions of clearance flow even though there are 6.5 times as many grid nodes in the gap for grid F as for grid C. As noted above, at 98% chord, the efficiency for grid C is 0.3 points lower than grids S and M, which can be attributed to the difference in the clearance mass flow rate. Analysis of the flow in the vicinity of the tip clearance gap indicated that the modeling of the gap employed in the single block cases, S and M, resulted in less pressure difference across the blade tip than in the blocked cases, C and F. This resulted in the lower mass flow rate through the tip clearance gap for the single block grids. In order to put these differences in predicted tip clearance mass flow rate into perspective, consider a modern impeller at about 4.5:1 pressure ratio and inlet mass flow rate of 4.5 kg/sec running with an axial tip clearance gap at the impeller exit of 0.254mm (0.010 inch), which is a reasonable value for this size machine. Since clearance flow varies directly with gap height the difference in the clearance flow rates predicted herein (about 1%) would translate to an uncertainty in the running clearance of 0.0025mm (0.001 inch) for the aforementioned impeller. Dynamic clearance measurements made by Skoch (1995) on a 4.5 kg/sec impeller indicated a 23% change in axial tip clearance when the mass flow rate changed by 10% from the design value at a constant rotational speed. Consequently, the uncertainty in accurately determining the tip clearance gap which directly influences the tip clearance mass flow rate is much larger than the differences noted between the different grid cases investigated herein. Therefore, from the standpoint of predicting the "absolute value" of the impeller performance the differences are insignificant. From the standpoint of predicting the "relative differences" all grids should predict the same trends.

With the observed differences in predicted tip clearance mass flow distributions shown in Fig. 7 in mind, the differences in the predicted distributions of pressure rise and work input shown in Fig. 6 are further explored. Although not discernible from Fig. 6, between 60–85% meridional chord the predicted pressure rise and work input of cases F and C decrease by about 1% relative to cases S and M. Since the only common difference between the single and multi-block cases is the predicted differences in tip clearance mass flow distributions (see Fig. 7), the changes in predicted pressure rise and work input that occur between 60–85% meridional chord are probably tied to the differences in predicted tip clearance mass flows. Most of the observed differences in the various predictions are tied to the differences in the trailing edge modeling which are made over the last 1.5% of meridional chord from the trailing edge. Cases S and M which produce the largest changes in predicted pressure rise and work input differ only in their trailing edge modeling, see Fig. 6. Therefore, the differences in tip modeling or gridding of the tip, at least from this one-dimensional perspective, appear to play a small role in contributing to the observed differences in predicted overall pressure rise and work input.

Axisymmetric Averaged Flow Field

Aside from the ability to predict overall performance it is important to be able to accurately predict the spanwise distribution of relevant flow quantities, or at the very least their relative shape and trends, in order for the predictions to provide guidance in the design of the compressor blades. Figures 8—11 show comparisons of the predicted and measured spanwise distributions of through-flow and absolute tangential velocities normalized by impeller exit tip speed at several meridional chord locations. The axisymmetric average velocities are calculated as pitchwise velocity weighted averages (density is assumed constant). As will be shown in the following discussion, up to about 90% meridional chord the variations in the solutions from the various grids are small, and are predominantly due to the differences in tip clearance mass flow. Downstream of 90% meridional chord the impact of the different trailing edge models or gridding becomes apparent. Again, the comparisons focus on differences between the single block cases and the multi-block case C.

The results in Fig. 8, at about 15% meridional chord, illustrate that all predictions, although different than the measured distribution, agree favorably with each other (cases S, M, C are generally within ±0.3%). At 89% meridional chord, Fig. 9, where the predicted one-dimensional pressure rise (see Fig. 6) starts to show marked differences between the four cases, the effect of differences in the clearance flow and trailing edge model or gridding are becoming apparent. The differences between the single block cases and case C is predominantly confined to the outer 40 % of span, within the influence of the through-flow wake. From 0 to 90% span case C is within ±3% of cases S and M which are essentially identical. Additional comparisons of contour plots of through-flow and absolute tangential velocity at 89% chord (not shown) show little differences between the four predictions in spite of the 1% increases in tip clearance mass flow for the multi-block predictions relative to the single block predictions. Differences within the through-flow wake region are evident, but the zone of influence of the through-flow wake is essentially unchanged. The major differences

between the multi-block case C and the single block cases at 89% chord is tied to their different clearance mass flow rates. An integration of entropy production from 0–40% span and from 40–100% span was done to assess the relative affects of the tip clearance flow. The cut off at 40% span was determined from inspection of the through-flow velocity contours at 89% chord which indicated that the through-flow velocity wake was confined to the outer 60% of span. For the lower 40% span there was no difference between cases S, M, and C. This provides confirmation that the tip clearance flow is responsible for the small decrement in efficiency for case C versus cases S and M.

At 99% meridional chord, Fig. 10, the relative differences in overall work input previously mentioned are supported by the observed differences in absolute tangential velocity profiles. These differences are a direct result of the differences in trailing edge geometry since at 89% chord (see Fig. 9) the tangential velocity distributions for S and M are identical. These rather large differences in predicted work input occur even though modifications to the trailing edge geometry are made over only the last 1.5% of meridional chord from the trailing edge.

Downstream of the impeller trailing edge at 109% meridional chord (1.065 radius ratio), Fig.11, the differences between the various predictions is slightly more pronounced than at 99% chord. Although there's no clear consensus that one grid case provides better predictions than another, the next section which describes blade-to-blade results indicates that case C does the best job of capturing certain blade-to-blade flow features that agree with the measurements as a result of gridding the trailing edge region. This may explain why the coarse multi-block solution, case C, which uses essentially the same grid as the single block cases, except for the additional tip clearance

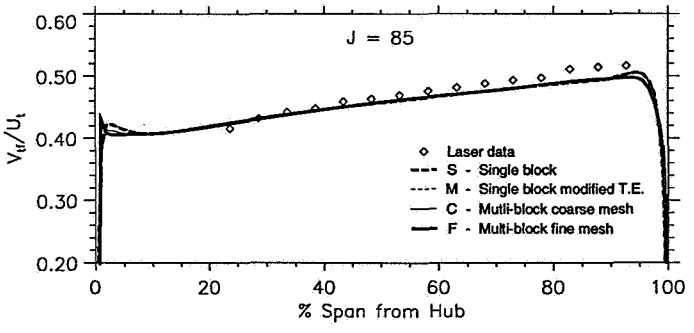

a) Through-flow velocity normalized by exit tip speed

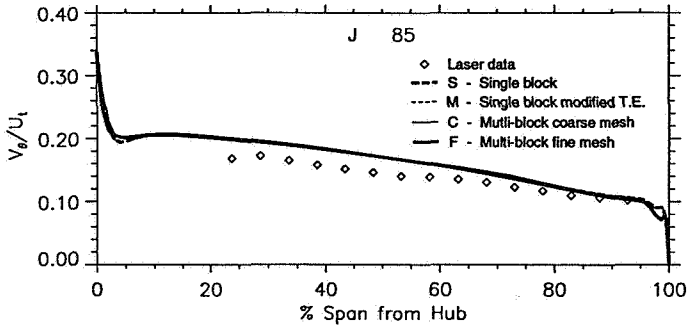

b) Absolute tangential velocity normalized by exit tip speed

Figure 8 Spanwise velocity distributions at station 85 (15% m/m$_s$).

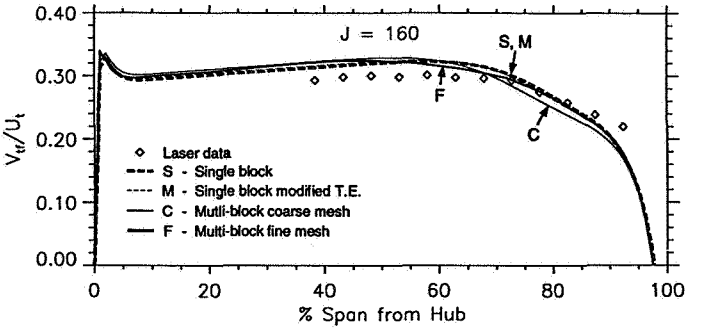

a) Through-flow velocity normalized by exit tip speed

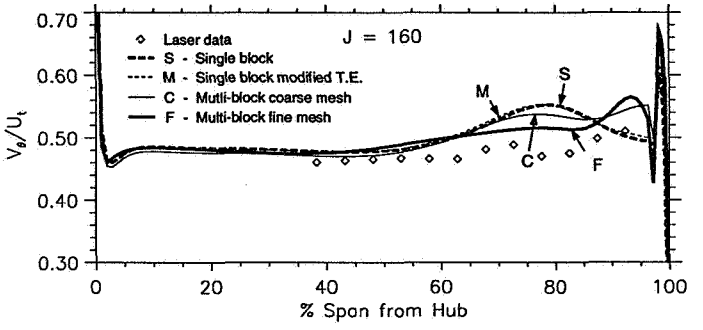

b) Absolute tangential velocity normalized by exit tip speed

Figure 9 Spanwise velocity distributions at station 160 (89% m/m$_s$).

gap and trailing edge blocks, comes closest to predicting the general character of the spanwise distribution of through-flow velocity at 1.065 radius ratio. The fine multi-block solution, case F, does no better than the single block solutions in predicting the spanwise distribution of through-flow velocity in spite of having almost twice the mesh. The best agreement with the measured spanwise distribution of tangential velocity is provided by the single-block predictions of case M. However, for this station it appears that the finer resolution of case F in the outer span region may be enabling a better prediction of the increase in tangential velocity near the casing. The reduced overall tangential velocity we attribute to lack of adequate grid resolution in the middle part of the channel. The spanwise distribution of tangential velocity at 1.065 radius ratio has been independently confirmed by pneumatic probe survey data (aero data), laser data, and hot-wire data (data are within ±4% of each other), and is very consistent with the comparison of one-dimensional work input shown in Fig. 6b.

Although there appears to be no consensus as to which case affords the best predictions, the multi-block codes which better define the geometry appear to show improvements in predicting certain flow features. The single block solutions do as good a job as the multi-block solutions for comparative analysis of designs. However, as indicated by the fine multi-block solution, case F, the improvements in predictive capability afforded by multi-blocking can be offset by insufficient gridding in regions of flow gradients. The fine multi-block solution mesh is coarser than the other cases from 10–85% span which is where the measurements are indicating some spanwise character in the through-flow velocity distribution. However, the hump in through-flow velocity evident in the data at around 80–85% span is somewhat better

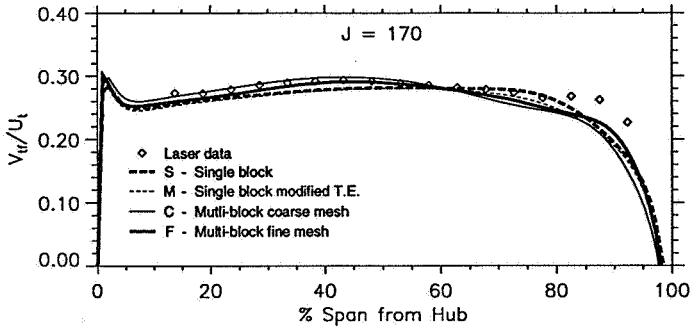

a) Through-flow velocity normalized by exit tip speed

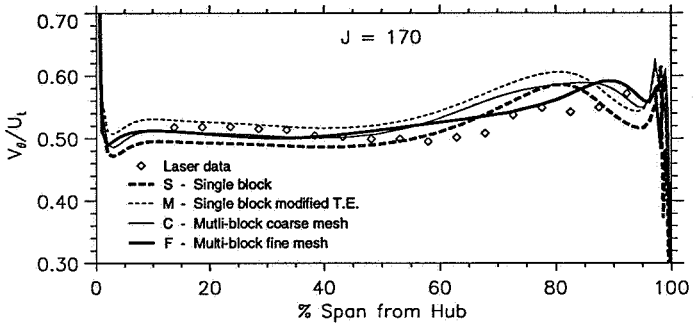

b) Absolute tangential velocity normalized by exit tip speed

Figure 10 Spanwise velocity distributions at station 170 (99% m/m_s).

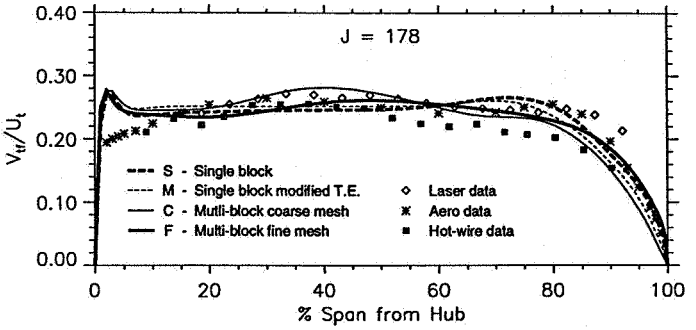

a) Through-flow velocity normalized by exit tip speed

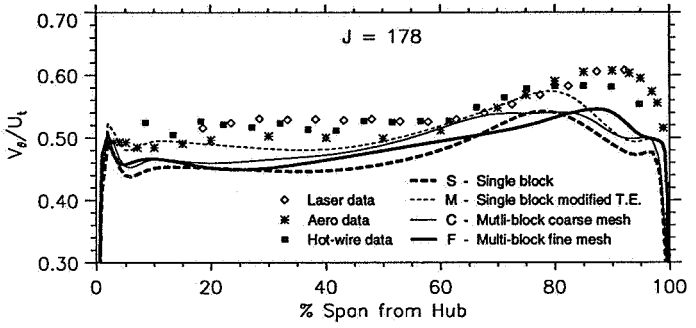

b) Absolute tangential velocity normalized by exit tip speed

Figure 11 Spanwise velocity distributions at station 178 (109% m/m_s, 1.065 r/r_t).

predicted by the fine multi-block solution, case F, which is exactly where the fine multi-block mesh density begins to increase. Case F has 16% more points total in the spanwise direction compared to the other cases, but 25% fewer mesh points in the spanwise direction from 10–85% span and 40% fewer from 55-85% span. Not surprisingly, the mesh distribution is as important as accurate modeling of the flow.

Blade-to-Blade Flow

The last area to consider is the details of the predicted blade-to-blade flow variations in the region where a designer might locate a diffuser. For example, the blade-to-blade details might be used to identify regions of accumulated low momentum fluid which could greatly alter the intended flow pattern and affect the diffuser performance. The ability to predict the blade-to-blade flow features implies better prediction of the fundamental flow physics and would suggest more confidence in the predictions of the spanwise and overall performance parameters.

Figure 12 compares contour plots of the measured and predicted distributions of through-flow velocity at 1.065 radius ratio. The multi-block cases show better qualitative agreement with the laser measurements whereas the single block cases are quite different in character. The predictions of the magnitude of the velocities near the blade wake and within and bounding the through-flow velocity wake show good comparison to measurements for the multi-block cases, particularly the coarse multi-block case, relative to the single block cases. The better agreement with measurements of the through-flow wakes predicted by the multi-block cases is in part due to the differences in predicted tip clearance mass flows relative to the single block cases (Fig. 7). Case C also resolves more details of the blade wake than the other cases. Further analysis of the solutions shows that the predominant difference of case C relative to the single block cases is the development of what appear to be two counter-rotating vortices in the "near streamwise direction" that form aft of the trailing edge and severely distort the wake fluid. These counter-rotating vorticies appear to be generated as a result of strong secondary flows which feed flow into the wake above and below about 40% span. This persists downstream and appears to give rise to the region of high through-flow velocity along the suction side of the wake at about 40% span, as depicted in the contour plots of Fig. 12 for both the case C predictions and the laser measurements. This may also explain why case C shows a slight increase in through-flow velocity, relative to the other cases, near about 40% span in Fig. 11a. Comparison of plots of the secondary velocity vectors (not shown) from the case C predictions with the laser measurements acquired at 1.02 radius ratio (station J=173) show good qualitative agreement. The laser measurements tend to confirm the predictions of case C since they also show flow moving into the wake in the same areas as those seen in the prediction. Again, due to inadequate spanwise mesh distribution, the fine multi-block solution, case F, does not do as good a job in predicting the flow character as the coarse multi-block solution It would have been better to place the increased grid points in the passage rather than in the tip gap (given that case F has over 6 times more grid points as case C within the tip clearance gap yet does no better than C in predicting the tip clearance flow). The two vortices meet near 50% span where the spanwise spacing for C is 5.7% of span (versus 7.6% for F). For C the edges of the vortices at

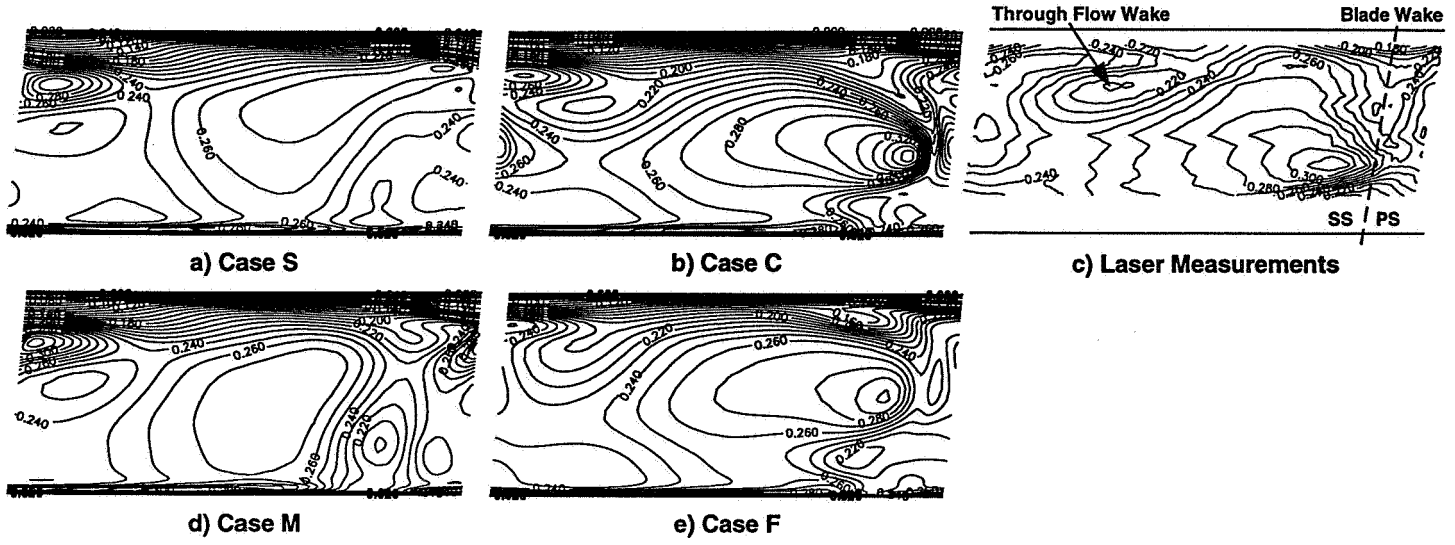

Figure 12 Comparison of predicted and measured distributions of through-flow velocity at station 178 ($r/r_t = 1.065$) normalized by exit tip speed, 153 m/s.

mid-span are not well-defined (i.e. there are only a few cells defining the interface of the two vortices). This would indicate that this spanwise spacing is marginal in terms of capturing spanwise flow details such as these. At this time, however, that conclusion is problematic and requires more exploration.

The extent to which the various cases predict the decay of absolute flow angle fluctuations indicates their potential for use in analysis of the unsteady impeller/diffuser interactions. Thus, the pitchwise variations in absolute flow angle fluctuations are shown in Fig. 13 and the magnitude of these fluctuations are tabulated in table 2 for 1.037 and 1.065 radius ratio at 40% and 90% span from the hub. Forty percent span is about the location where C yields a high value of through-flow velocity in Fig. 12 and 90% span is in the through-flow wake. For 90% span and 1.037 radius ratio C and F predict a double peak indicative of the blade wake and the through-flow wake whereas S and M predict only one peak. The agreement of C and F at this location compared to the laser data is quite good. At 40% span and 1.037 radius ratio C produces a very strong wake angle fluctuation that is twice as large as the measured values (see table 2). Case F does not produce this large swing, but in this region the spanwise grid spacing for F is much coarser than it is for C and, thus, could contribute to some smearing of the flow. At 90% span and 1.065 radius ratio, F is the only one of the four cases to produce the double peak measured and may be indicative of the greater pitchwise mesh density of F in this region. A plot of all spanwise locations (not shown) indicated that by a radius ratio of 1.08, the flow angle fluctuations for all solutions are below 15 degrees, and by 1.2 radius ratio the flow angle fluctuations are less than 12 degrees. If one looks at all percent span locations there is not a clear choice as to which grid yields the best results and further work needs to be done to determine what factor is most important in predicting the correct magnitude of the flow angle variation.

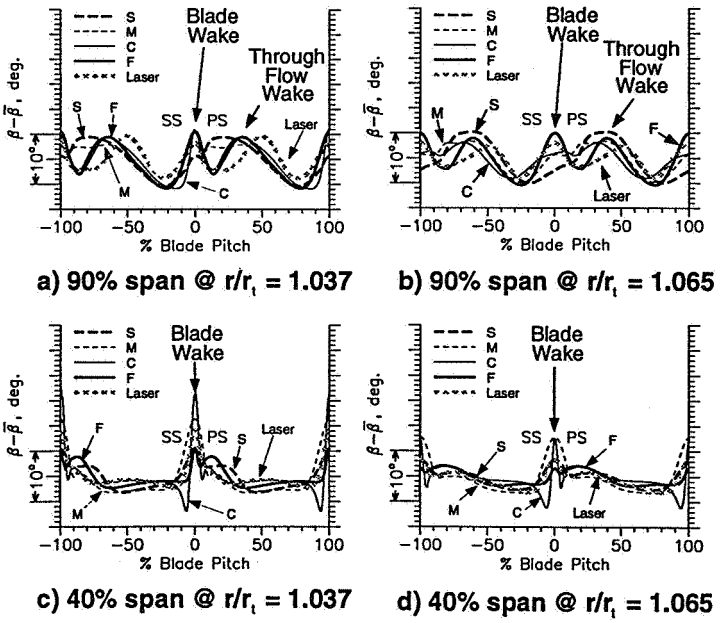

Figure 13 Pitchwise distribution of absolute flow angle variation, $\beta - \bar{\beta}$, in the vaneless diffuser.

Relative "Costs" of Analyses

Table 3 provides a comparison of the relative "costs", in terms of CPU time and memory requirements, of running the various cases. The basis for comparison is the single block solution, case S. The benchmark results provided in table 3 were obtained using the NASA LACE cluster, a network of IBM RS/6000 Model590 computers. As previously mentioned, all cases, whether single or multi-block were run as multi-block jobs in order to take advantage of ADPAC's parallel execution capability which parallelizes a job according to it's multiple block structure. The single block cases were each run using 3 equally loaded processors (in terms of number of mesh nodes per processor). The multi-block cases were run two ways: 1) with the minimum number of equally loaded processors required for each to

be loaded similar to the single block cases, and 2) with three equally loaded processors as in the single block cases. The rationale behind the comparisons were to both try to assess the relative CPU time as a result of increased number of grid nodes (and not due to any differences which might occur as a result of one processor being more heavily loaded than another), and to assess the relative CPU time due to increased processor loading as a result of additional grid nodes required for the multi-block cases. Although not measured, there was an additional perceived penalty for the multiple-block cases which seemed to require more iterations to achieve convergence, roughly proportional to the increased time per iteration for the comparatively loaded processors (i.e., case F using 6 processors required roughly 40% more iterations as case S to converge from a given perturbation in back pressure).

Table 2 Magnitude of absolute flow angle fluctuations in the vaneless diffuser, in degrees.

% Span from Hub	Case	r/r_t	
		1.037	1.065
40	S	9	6
	M	15	11
	C	24	14
	F	8	4
	Laser	12	7
90	S	10	11
	M	9	9
	C	12	8
	F	12	11
	Laser	7	8

Table 3 Comparison of computer resources in terms of CPU time and memory requirements.

CASE	NUMBER OF PROCESSORS	RELATIVE MEMORY PER PROCESSOR	RELATIVE CPU TIME PER ITERATION
S	3	1.000	1.000
M	3	1.000	1.002
C	4	0.909	1.083
	3	1.114	1.164
F	6	0.980	1.408
	3	1.993	2.052

SUMMARY OF RESULTS

The focus of the paper is to identify areas of interest in a design mode where a designer could use a single block grid for a Navier-Stokes solver with some modeling of the true geometry versus a more complicated multi-block grid that better models the actual geometry of the turbomachine under consideration. Our intent was to focus on one-dimensional overall parameters, pitchwise averaged spanwise variations, and the complete flowfield which would indicate the level of interest the designer had in the details of the machine being analyzed. Of the four solutions presented it is not possible to conclude that one particular grid always gives better results since, depending upon the flow feature of interest, some agree with the data better for some features and others agree better with the data for other features. However, we can state that if one is interested in prediction of overall performance numbers, whether the tip gap is modeled (cases S and M) or gridded (cases C and F), the results are the same within an acceptable level of accuracy (±0.5% in pressure ratio and ±1 point in efficiency). This same statement is also true for the spanwise distributions and the details of the flow. The different predicted tip clearance flow between the modelled cases (S and M) and the gridded cases (C and F) - one percent of inlet flow - does not alter the results to any significant degree.

Modeling of the trailing edge, however, produces significant differences between both the single block cases (S and M) and the multi-block cases (C and F) for the overall work input and pressure ratio. Whether one models the trailing edge as a tapering of both sides of the blade to the mean camber line (S) or as a taper of the suction surface to the pressure surface (M) results in about a 7% difference in work input with the M solution being less than 1% below the experimental value of work input. A comparable difference exists in pressure rise with M being 2% higher than the measured value. Both multi-block solutions under predict the work input by about 5% of the measured value and predict the pressure rise correctly for case C and 1% low for case F. The differences in work input begin at about 90% chord (recall the modification of the trailing edge began at 98.5% chord so there is considerable upstream influence of the trailing edge) and persists downstream. Case C resolves more flow details of the through-flow velocity at a radius ratio of 1.065 than the others in part because of two counter-rotating vortices that form aft of the trailing edge and severely distort the wake fluid. In terms of predicted wake decay, there is little difference in how the wake decays. All solutions predict most of the wake decay occurs before the 6.5% radius ratio and that setting a diffuser beyond that radius ratio would not decrease flow angle swings into the diffuser by a significant amount. Near the trailing edge the magnitude of the angle swing is greatly dependent upon the modeling of the trailing edge, but by 8% radius ratio all the cases predict angle swings less than 15 degrees (this considers all percent span locations) and not much reduction occurs beyond that radius ratio.

CONCLUSIONS

Although none of the grids investigated produced superior results in every case when compared to the measurements, in general, we can say that grid C which added coarse gridding to the tip gap region and a blocked grid downstream of the trailing edge yielded the best results. However, the results from F indicate that increased grid density away from the hub and tip may improve the results from C. In summary we conclude the following:

1. Increasing grid density in the tip gap by a factor of 6.5 resulted in no difference in predicted tip clearance overall flow nor in the chordwise distribution of the clearance flow. A fairly coarse grid as used in C seems perfectly adequate. Also, the modeling used in the single block grids gives results that are quite good, especially if one is doing comparative studies. For analysis cases the difference in tip clearance mass flow rate between the modeled and gridded cases is well within the uncertainty of the actual tip clearance gap height.
2. Blocking the trailing edge with a grid so the trailing edge geometry is properly modeled reduces uncertainties in how to taper the blade to zero thickness if using a single block code but appears to offer no great benefit for the present case although some details of the flow downstream of the impeller are better predicted. However, we caution that more cases need to be investigated before we would offer this as a more general conclusion.
3. Since the trailing edge treatment used for a single block code can significantly affect the results, we would recommend using a multi-block code. If a multi-block code is not available, we recommend using the blade trailing edge taper for grid S since it produces the same type of pressure and temperature rise behavior near the trailing edge as produced with C. However, we would suggest a more gradual taper than used in S to reduce any spurious entropy rise due to high grid shear. It may also be better to make a more symmetric taper around the mean camber line based upon normal thickness taper rather than tangential thickness taper as done for S. This may inhibit the tendency of the flow to turn rapidly around the pressure surface with the resultant under turning of the flow.
4. For this case, in order to capture the spanwise details measured with the laser downstream of the trailing edge, it appears that a grid spacing of 5.7% span at mid span is marginal and should be reduced in order to resolve the local gradients.
5. The choice of grids for the trailing edge yields considerable differences in the swings in the pitchwise absolute flow angle near the trailing edge. However, all four grids predict swings less than 15 degrees by an 8% radius ratio and none predict much decrease beyond that radius.

ACKNOWLEDGMENTS

The authors are grateful to Dr. Ed Hall, and Nathan Heidegger at Allison Engine Co. and Dr. Chris Miller at NASA's Lewis Research Center for their helpful suggestions and assistance regarding the ADPAC analyses. The authors are also grateful for the suggestions of Dr. Ali Ameri of the University of Kansas Center for Research Inc., Resident Research Associate, NASA Lewis Research Center.

REFERENCES

Adamczyk, J. J., 1995, private communication.

Baldwin, B. S., and Lomax, H. 1978, "Thin-Layer Approximation and Algebraic Model for Separated Turbulent Flows," AIAA Paper 78–257, 1978.

Chriss, R. M., Hathaway, M. D., and Wood, J. R., 1994, "Experimental and Computational Results from the NASA Lewis Low-Speed Centrifugal Impeller at Design and Part Flow Conditions," ASME Paper 94–GT-213, accepted for publication in the Transactions of the ASME.

Hall, E. J. and Delaney, R. A., 1992, "Investigation of Advanced Counterrotation Blade Configuration Concepts for High Speed Turboprop Systems: Task V — Counterrotation Ducted Propfan Analysis, Final Report", NASA CR 187126, NASA Contract NAS3–25270.

Hall, E. J. Topp, D. A., Heidegger, N. J., and Delaney, R. A., 1994, "Investigation of Advanced Counterrotation Blade Configuration Concepts for High Speed Turboprop Systems: Task VIII — Cooling Flow/Heat Transfer Analysis, Final Report", NASA CR 195360, NASA Contract NAS3–25270.

Hathaway, M. D., Wood, J. R., Wasserbauer, C. A., 1992, "NASA Low Speed Centrifugal Compressor for 3-D Viscous Code Assessment and Fundamental Flow Physics Research," ASME Journal of Turbomachinery, Vol. 114, April 1992, pp. 295–303.

Hathaway, M. D., Chriss, R. M., Wood, J. R., Strazisar, A. J., 1993, "Experimental and Computational Investigation of the NASA Low-Speed Centrifugal Compressor Flow Field," ASME Journal of Turbomachinery, Vol. 115, No. 3, July 1993, pp. 527–542.

Hathaway, M. D., Chriss, R. M., Wood, J. R., Strazisar, A. J., 1995, "Laser Anemometer Measurements of the Three-Dimensional Rotor Flow Field in the NASA Low-Speed Centrifugal Compressor," NASA TP-3527.

Jameson, A., Schmidt, W., and Turkel, E., 1981, "Numerical Solutions of the Euler Equations by Finite Volume Methods Using Runge-Kutta Time-Stepping Schemes," AIAA Paper 81–1259.

Skoch, G. J., 1995, private communication.

Strazisar, A. J., Wood, J. R., Hathaway, M. D., and Suder, K. L., 1989, "Laser Anemometer Measurements in a Transonic Axial-Flow Fan Rotor," NASA TP-2879.

Wood, J. R., 1994, private communication.

Wood, J. R., Adam, P. W., and Buggele, A. E., 1983, "NASA Low-Speed Centrifugal Compressor for Fundamental Research," NASA TM 83398.

REPORT DOCUMENTATION PAGE

Form Approved
OMB No. 0704-0188

1. AGENCY USE ONLY (*Leave blank*)	2. REPORT DATE	3. REPORT TYPE AND DATES COVERED
	March 1996	Technical Memorandum

4. TITLE AND SUBTITLE
Application of a Multi-Block CFD Code to Investigate the Impact of Geometry Modeling on Centrifugal Compressor Flow Field Predictions

5. FUNDING NUMBERS
WU–505–62–52
1L161102AH45

6. AUTHOR(S)
Michael D. Hathaway and Jerry R. Wood

7. PERFORMING ORGANIZATION NAME(S) AND ADDRESS(ES)
NASA Lewis Research Center
Cleveland, Ohio 44135–3191
and
Vehicle Propulsion Directorate
U.S. Army Research Laboratory
Cleveland, Ohio 44135–3191

8. PERFORMING ORGANIZATION REPORT NUMBER
E–10178

9. SPONSORING/MONITORING AGENCY NAME(S) AND ADDRESS(ES)
National Aeronautics and Space Administration
Washington, D.C. 20546–0001
and
U.S. Army Research Laboratory
Adelphi, Maryland 20783–1145

10. SPONSORING/MONITORING AGENCY REPORT NUMBER
NASA TM–107198
ARL–TR–876

11. SUPPLEMENTARY NOTES
Prepared for the 41st Gas Turbine and Aeroengine Congress, sponsored by the International Gas Turbine Institute of the American Society of Mechanical Engineers, Birmingham, United Kingdom, June 10–13, 1996. Michael D. Hathaway, Vehicle Propulsion Directorate, U.S. Army Research Laboratory, NASA Lewis Research Center and Jerry R. Wood, Lewis Research Center. Responsible person, Michael D. Hathaway, organization code 2640, (216) 433–6250.

12a. DISTRIBUTION/AVAILABILITY STATEMENT
Unclassified - Unlimited
Subject Category 07
This publication is available from the NASA Center for AeroSpace Information, (301) 621–0390.

12b. DISTRIBUTION CODE

13. ABSTRACT (*Maximum 200 words*)
CFD codes capable of utilizing multi-block grids provide capability to analyze the complete geometry of centrifugal compressors including, among others, multiple splitter rows, tip clearance, blunt trailing edges, fillets, and slots between moving and stationary surfaces. Attendant with this increased capability is potentially increased grid setup time and more computational overhead - CPU time and memory requirements - with the resultant increase in "wall clock" time to obtain a solution. If the increase in "difficulty" of obtaining a solution significantly improves the solution from that obtained by modeling the features of the tip clearance flow or the typical bluntness of a centrifugal compressor's trailing edge, then the additional burden is worthwhile. However, if the additional information obtained is of marginal use then modeling of certain features of the geometry may provide reasonable solutions for designers to make comparative choices when pursuing a new design. In this spirit a sequence of grids were generated to study the relative importance of modeling versus detailed gridding of the tip gap and blunt trailing edge regions of the NASA large low speed centrifugal compressor for which there is considerable detailed internal laser anemometry data available for comparison. The results indicate: 1) There is no significant difference in predicted tip clearance mass flow rate whether the tip gap is gridded or modeled. 2) Gridding rather than modeling the trailing edge results in better predictions of some flow details downstream of the impeller, but otherwise appears to offer no great benefits. 3) The pitchwise variation of absolute flow angle decreases rapidly up to 8% impeller radius ratio and much more slowly thereafter. Although some improvements in prediction of flow field details are realized as a result of analyzing the actual geometry there is no clear consensus that any of the grids investigated produced superior results in every case when compared to the measurements. However, if a multi-block code is available it should be used as it has the propensity for enabling better predictions than a single block code which requires modeling of certain geometry features. If a single block code must be used some guidance is offered for modeling those geometry features which can't be directly gridded.

14. SUBJECT TERMS	15. NUMBER OF PAGES
Centrifugal; Compressor; Low speed; Computational; Laser anemometer	14
	16. PRICE CODE: A03

17. SECURITY CLASSIFICATION OF REPORT	18. SECURITY CLASSIFICATION OF THIS PAGE	19. SECURITY CLASSIFICATION OF ABSTRACT	20. LIMITATION OF ABSTRACT
Unclassified	Unclassified	Unclassified	